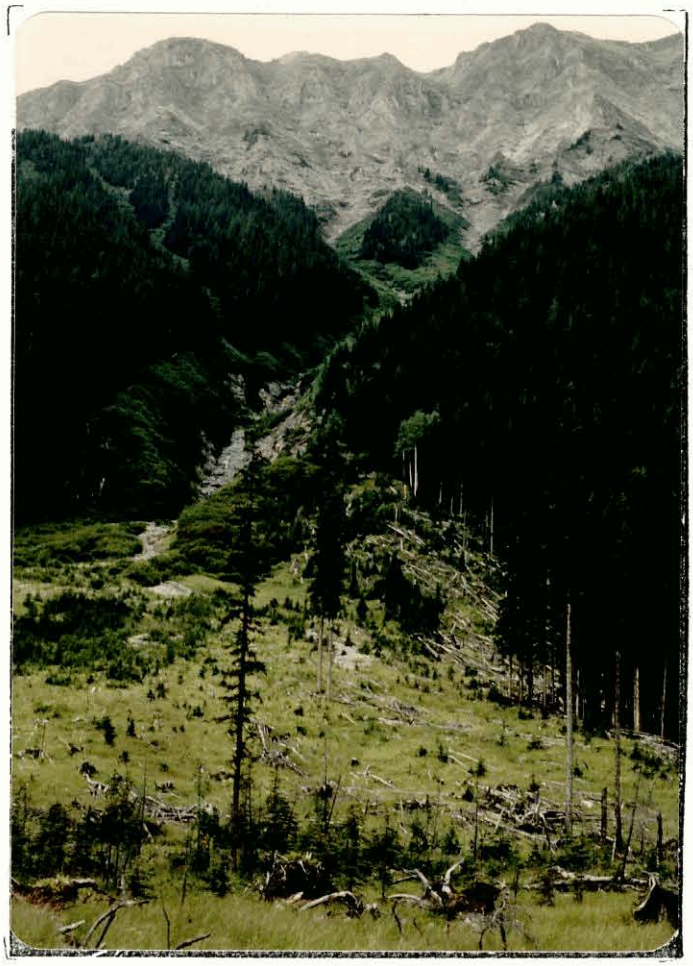

Figure 9

Aquila Ridge. The Ottertail Formation forms a cliff band above the roof of the complex along the ridge; the approximate locations of this contact and that between ijolitic rocks and the syenite breccia are drawn in. Further north (to the right) the syenite pinches out and ultramafic rocks are in direct contact with the limestone.

Figure 10

Tabular body of equigranular ijolite in urtitic pegmatite, Aquila Ridge. The hammer is lying just below the contact. Although such bodies superficially resemble dikes, they are invariably horizontal, and do not display features indicating an intrusive relationship, such as viening or brecciation. They may have resulted from convective cells arising from non-equilibrium chemical, thermal, and density gradients.

Figure 11

Cyclic layering in ijolite, Aquila Ridge. The irregular black band is a late lamprophyre dike, which cuts the lower contact of a symmetrically layered dike. Pale layers are rich in nepheline; dark layers in hedenbergitic pyroxene. The non-conforming layering above the dike contains pyroxene crystals visibly oriented perpendicular to the layering.

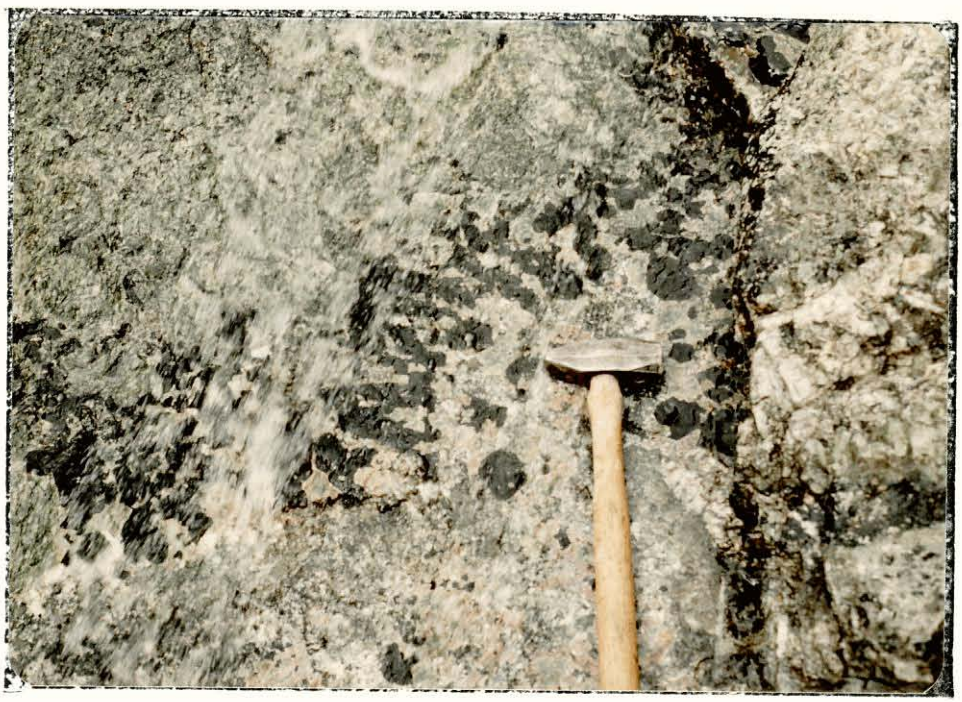

Figure 12

Pegmatitic pyroxene, Aquila Ridge. Such features are extremely common in the ijolites, and may reflect local concentrations of volatile constituents. The pegmatitic horizons frequently define a weak subhorizontal layering.

Figure 13

Nepheline rich pegmatite body in ijolite, Aquila Ridge. Such bodies likely resulted from dilatory expansion in a near-solid crystal mush.

Figure 14

Crescumulate layering in ijolite, Aquila Ridge. Although unfortunately not apparent from this photograph, the acicular pyroxene crystals extend down to the brown-black weathering band at the bottom of the picture, which is rich in magnetite and perovskite. Such textures likely resulted from very strong negative gradients in pyroxene forming components extending sideways from the crystals, forcing them to grow upward into more mafic portions of the liquid.

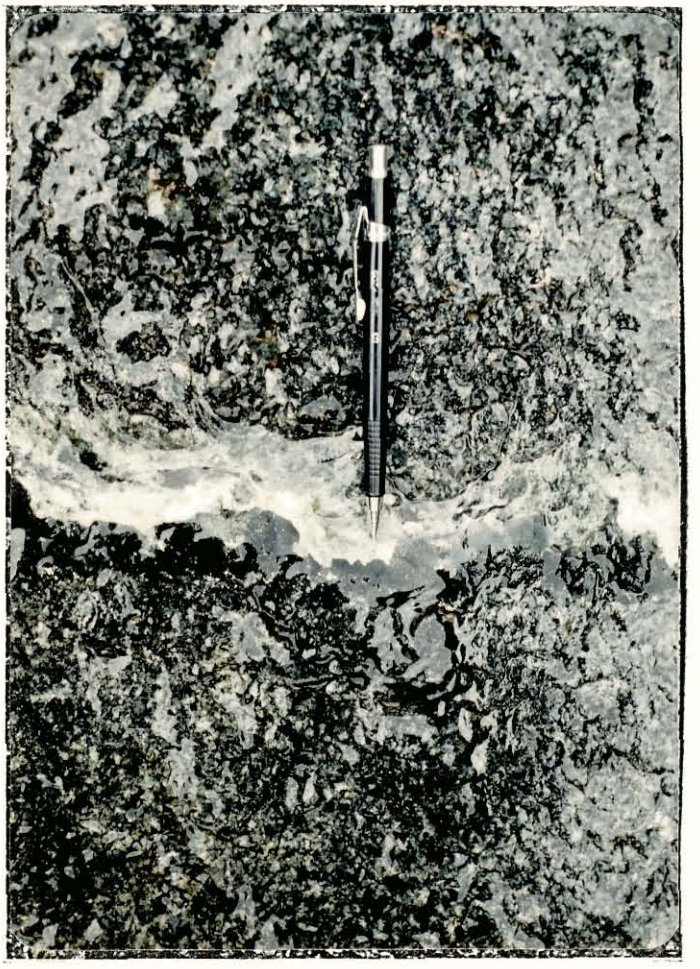

Figure 15

Melanite-zeolite layer in a tabular ijolite body, Aquila Ridge. The dark melanite has nucleated on mafic minerals, with the zeolitic layer (grossular-natrolite-pectolite) crystallizing above it. This has been interpreted to be the result of late stage liquid immiscibility, possibly a non-equilibrium process involving a chemical oscillator.

Figure 16

Isotropic ijolite, Aquila Ridge. This texture is extremely common in the ultramafic rocks, and indicates that gravitative accumulation of crystals was not a significant process during solidification. To the contrary, it would appear that the magma was too viscous to permit sedimentation, and the crystals were suspended during growth.

Figure 17

Euhedral diopside in titanaugite (sample 81-IR-6). Although anhedral diopside occurs with melanite (cf. figure 18), the presence of these crystals and of nodules of diopside in some ijolites and lamprophyres is difficult to explain. They may be a liquidus phase formed at high pressures, and present in the melt when it intruded into upper levels.

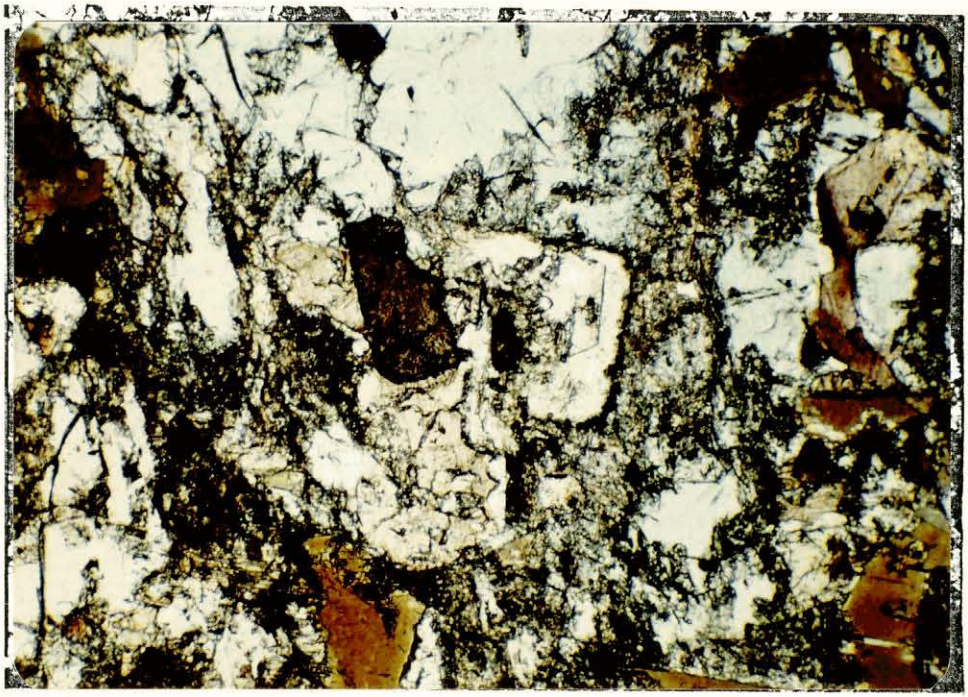

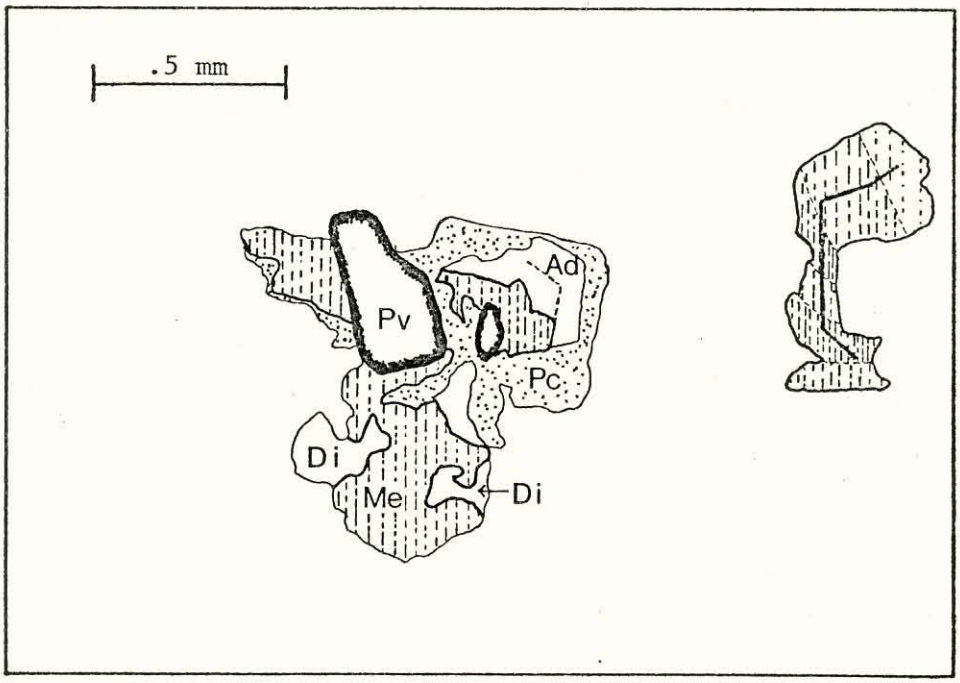

Coexisting iron-rich (melanite-diopside) and alkaline (andradite-pectolite) residua in a cavity in titanaugite. This texture implies late stage liquid immiscibility and a solvus between the two garnet compositions. Sample 81-IR-6.

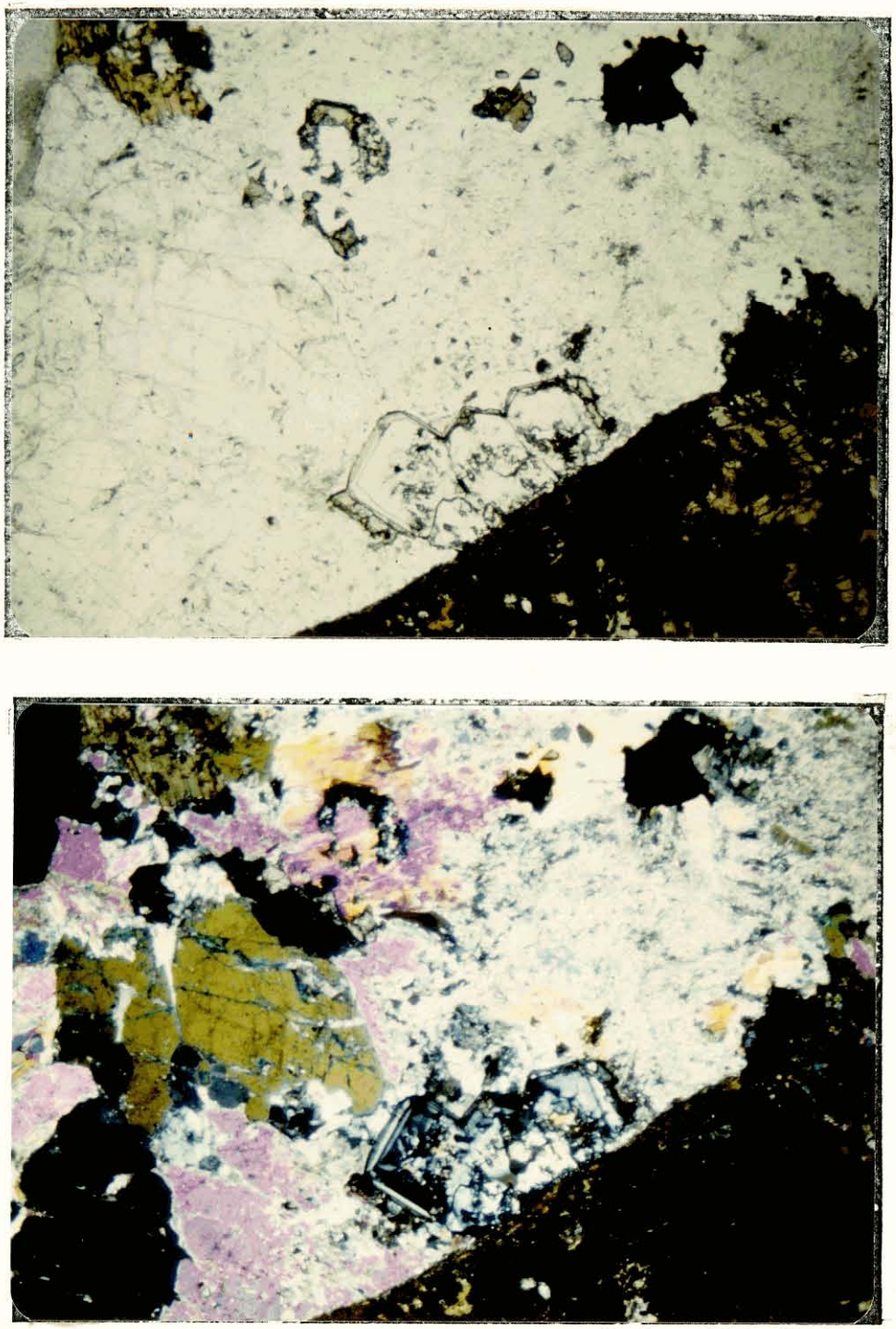

Figure 19

A large cavity occupied by basic residual minerals (81-IR-6). Although the formation of the liquid solidifying within such cavities is directly related to the formation of the residual Fe, Ti rich liquid (melanite) by mutual immiscibility, they are rarely found in contact. Nt=natrolite; Pc=pectolite; Cn=cancrinite; Sp=sphene, Ad=andradite.

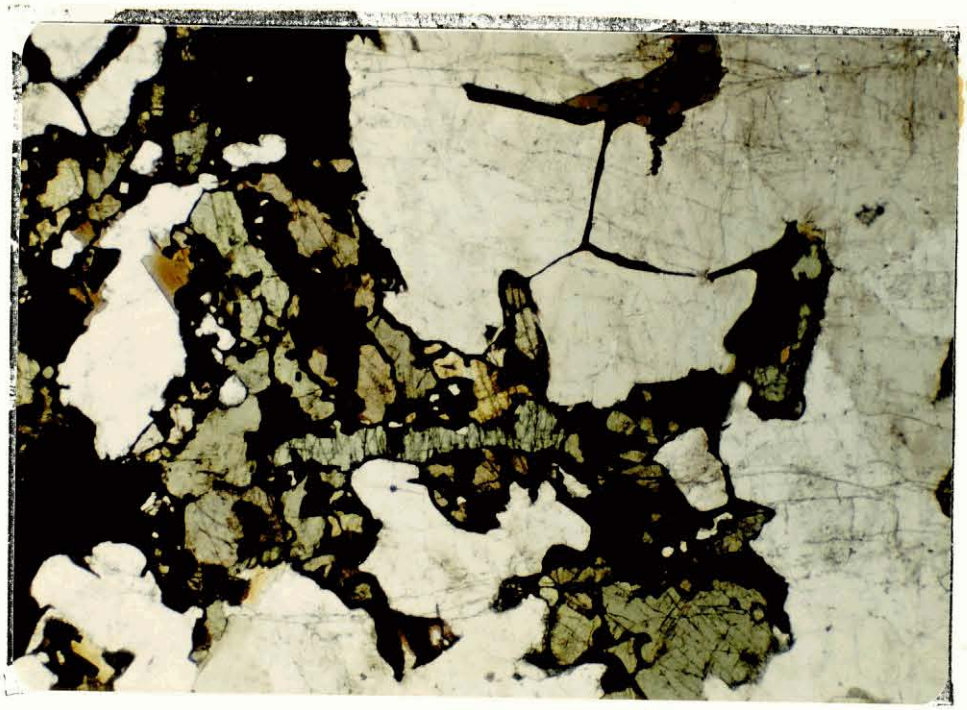

Figure 20

(82-IR-17)

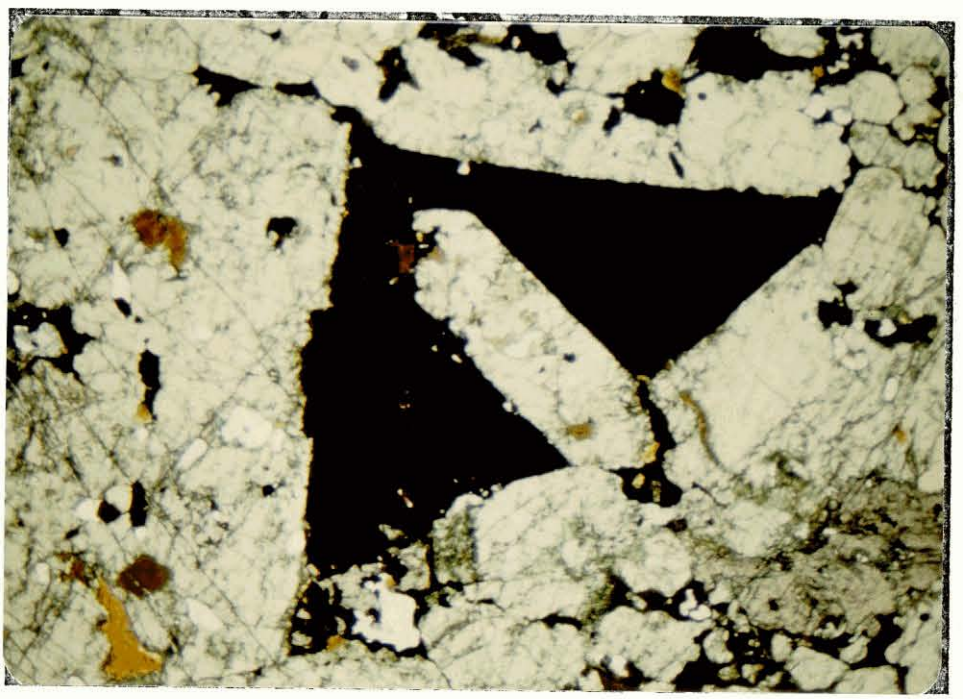

Figure 21

(82-IR-15)

"Wetting" and interstitial melanite textures in ijolites. These textures indicate the melanite originated as a discrete iron rich liquid, which precipitated preferentially on mafic minerals, particularly pyroxene.

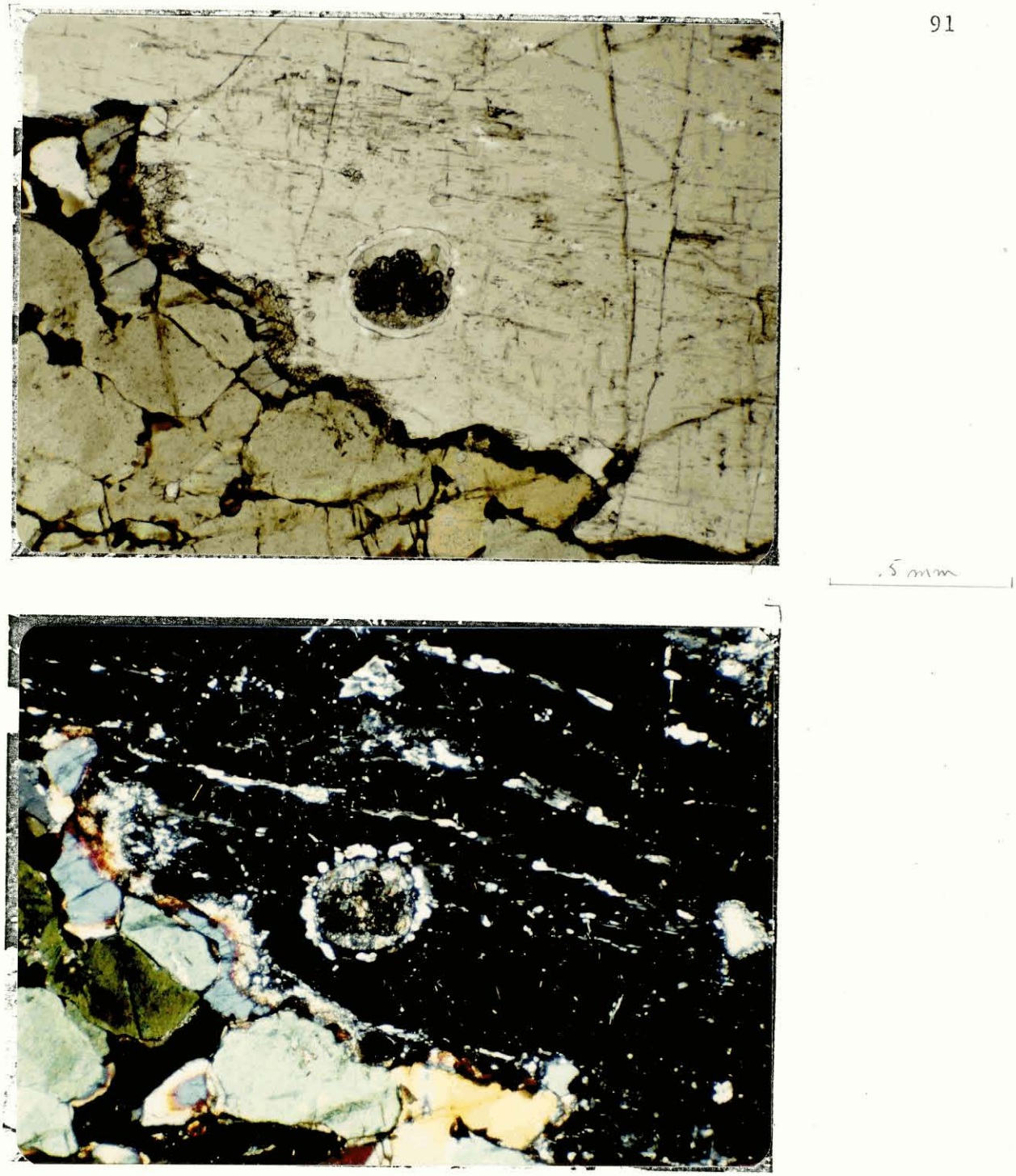

Figure 22

Globule of basic liquid trapped in nepheline (81-IR-8). The presence of aegirine (Ae) is a common variation of this material, indicating a transition from basic to more alkaline compositions. A thin rim of cancrinite developed from reaction with the host nepheline.

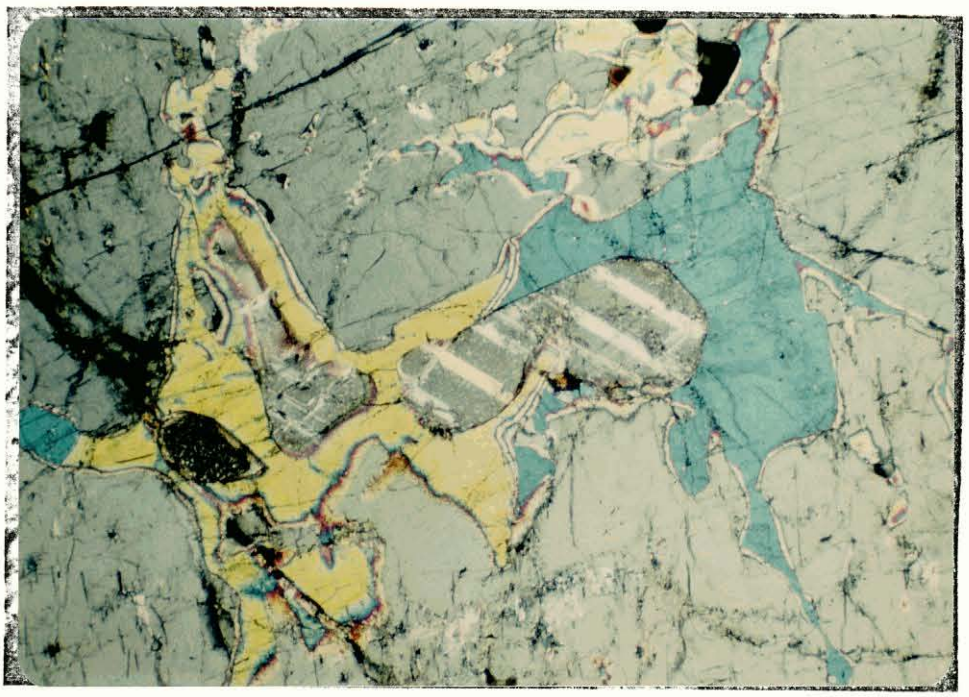

Figure 23

Calcite and cancrinite in urtite (81-IR-9). A reaction rim around calcite grains enclosed by nepheline is a very common texture in all ultramafic rocks, but particularly in urtites.

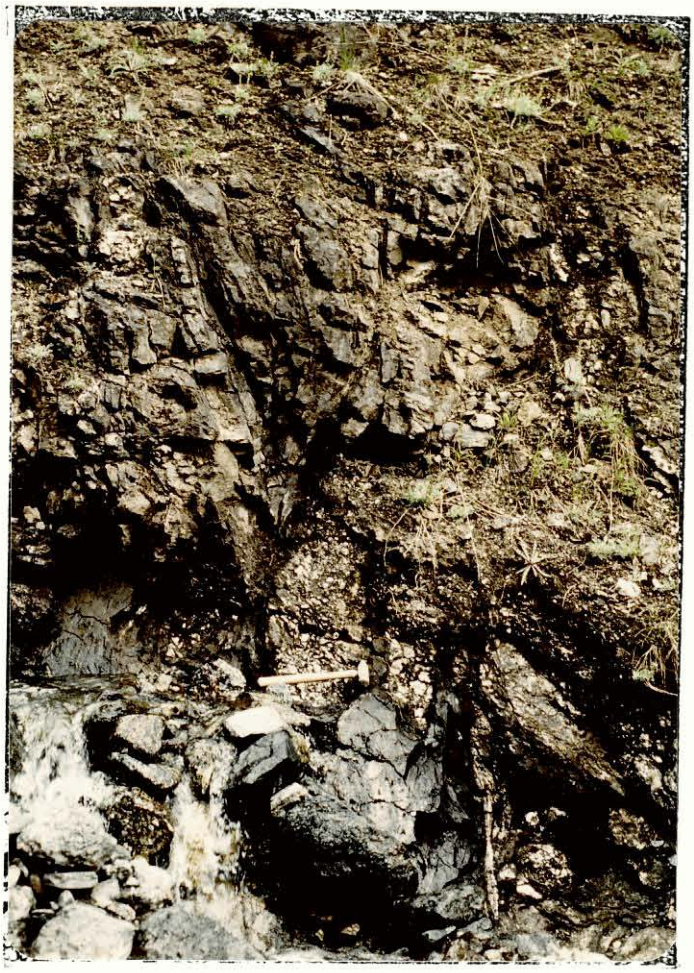

Figure 24

Dikes of black silicocarbonatite in biotite melteigite, Aquila Ridge. Such dikes are strongly flow-banded and contain large euhedral perovskite, an important liquidus phase of the contiguous ultramafic rocks.

Figure 25

Dike of red weathering carbonatite (left) intruding the buff weathering type. The latter is a calcite rich differentiate of the black carbonatite, presumably by liquid immiscibility. Evidence for this is found as discrete, elliptical bodies of buff in black, with very sharp contacts. Their relationship to the red variety is uncertain.

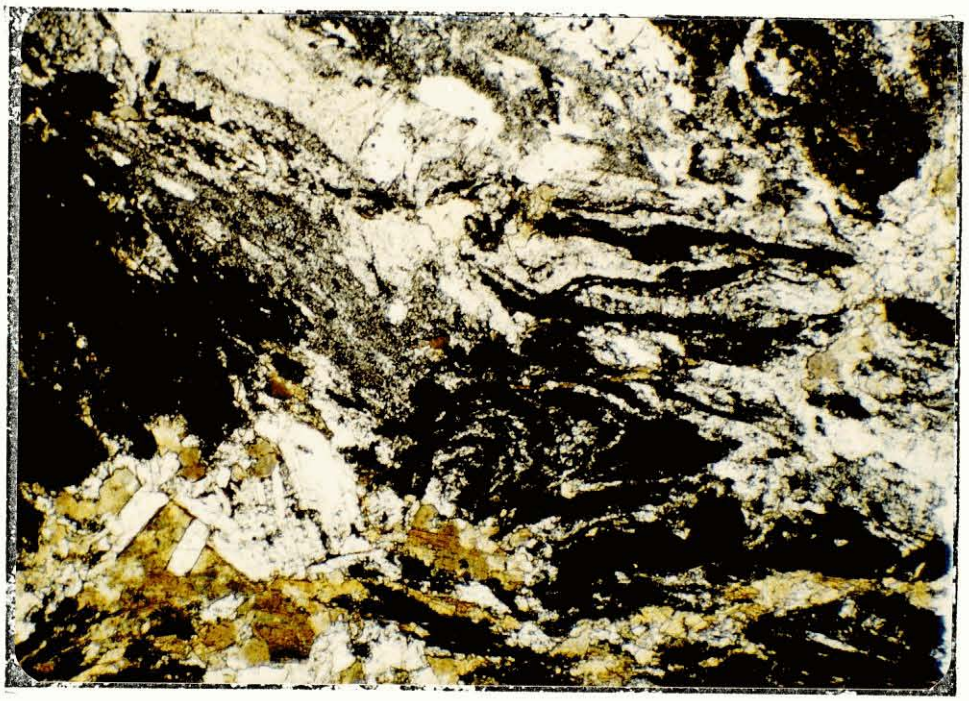

Figure 26

Flow banding in the base of a silicocarbonatite dike (83-IR-3). The opaque material is amorphous elemental carbon in a matrix of tetranatrolite; green berthierine and iron rich biotite occur in interstices between laths of calcite in the lower left corner.

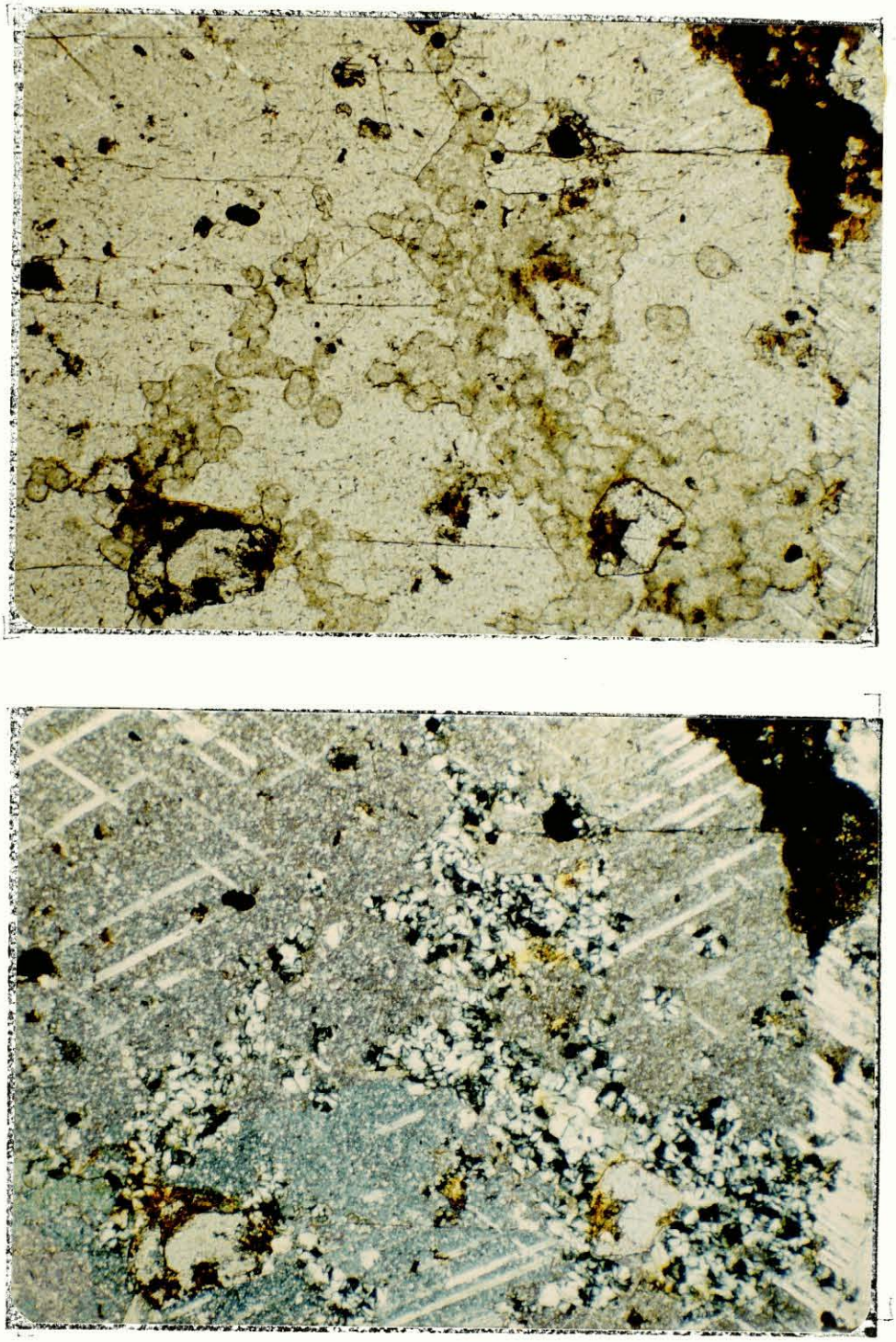

Figure 27

Berthierine globules in a calcite segregation in silicocarbonatite (83-IR-3). Such features are common, and reinforce the impression of continuing immiscibility between a silicate liquid and the carbonatite.

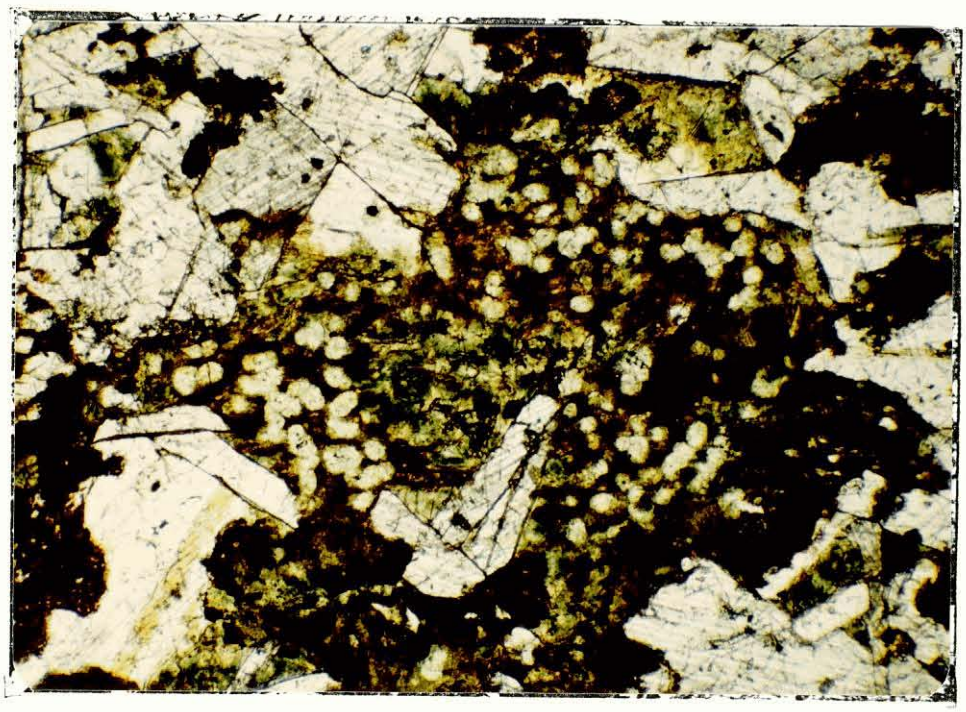

Figure 28

Berthierine globules with unidentified iron oxides, occupying a large interstitial cavity in manganese rich calcite. Large numbers of aegirine needles are visible in the calcite (83-IR-3).

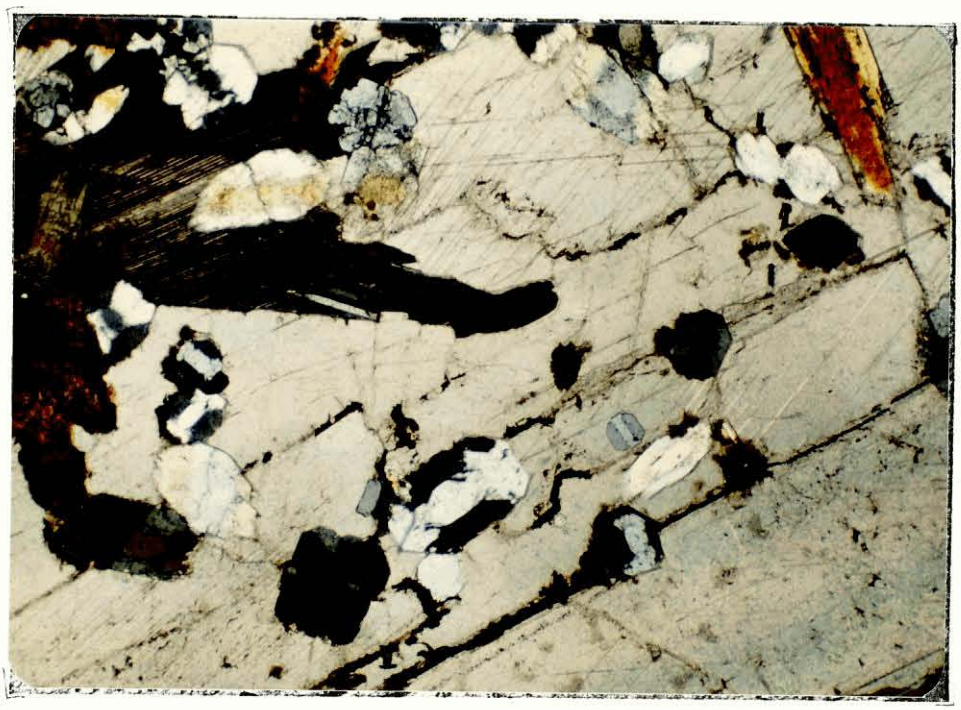

Figure 29

Natrolite crystals in silicocarbonatite (83-IR-5). The twinning is on (110), which produces an interesting pattern on sections perpendicular to the crystallographic C axis.

Figure 30

Breccia of cumulate jacupirangite in pale nepheline syenite, Buttress Peak. The photograph was taken approximately 5 feet above the contact, which is covered.

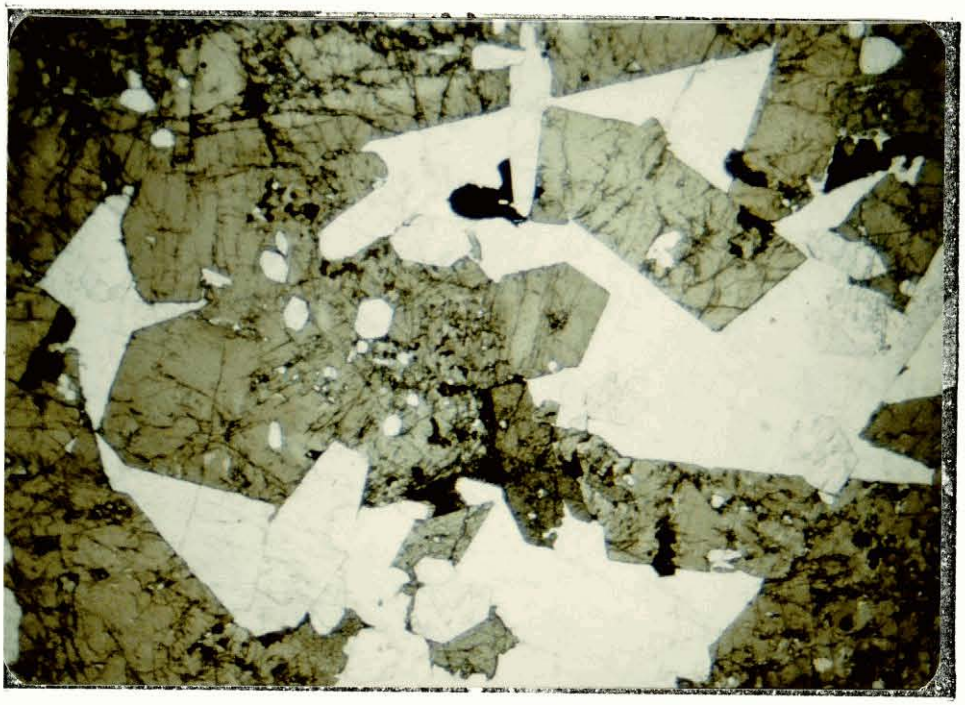

Figure 31

Highly idiomorphic titanaugite crystals in jacupirangite (82-MC-1C). Such idiomorphism is very rare in ijolites not near the contact, and indicates a cumulate origin for the pyroxenite. The amount of nepheline in this view (selected to display the idiomorphism) is anomalously large.

Figure 32

Syenite breccia with sedimentary inclusion, Buttress Peak. Three generations of syenite can be seen. The lower photograph is a closeup of the area outlined in the upper one, and shows the prominent layering in the first two intrusions and the coarse-grained, isotropic texture of the pale nepheline syenite.

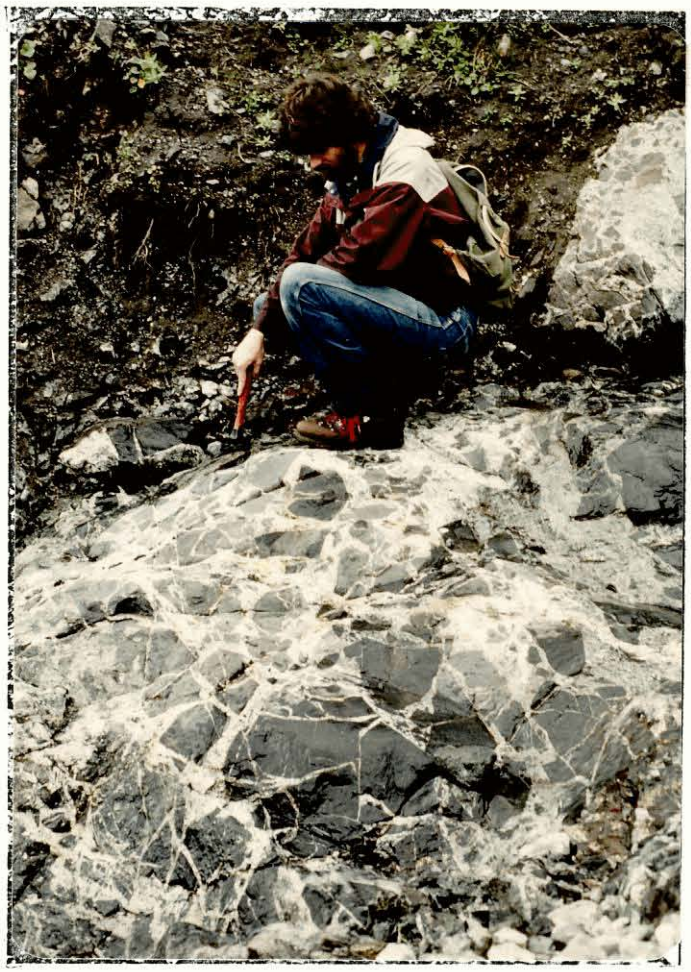

Figure 33

Syenite breccia, Buttress Peak.

Figure 34

Syenite breccia, Aquila Ridge. The exact same rock types are present at Buttress Peak, 7 kilometres distant (cf. figures 32,33).

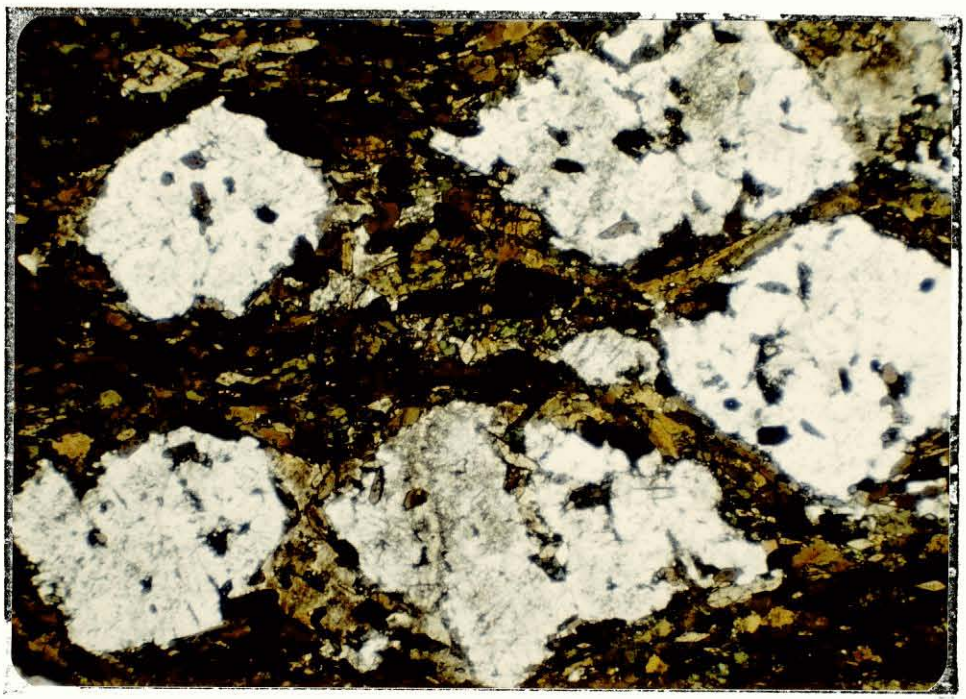

Figure 35

Amphibole jacupirangite (83-IR-7). The pale ocelli are aggregates of nepheline and sphene, in a matrix of kaersutite, pyroxene, and sphene. The origin of the very regulary spaced ocelli is uncertain, but their presence argues against an accumulative mechanism as causing the prominent layering in the matrix, and an origin related to cyclic layering in the ultramafic rocks is likely.

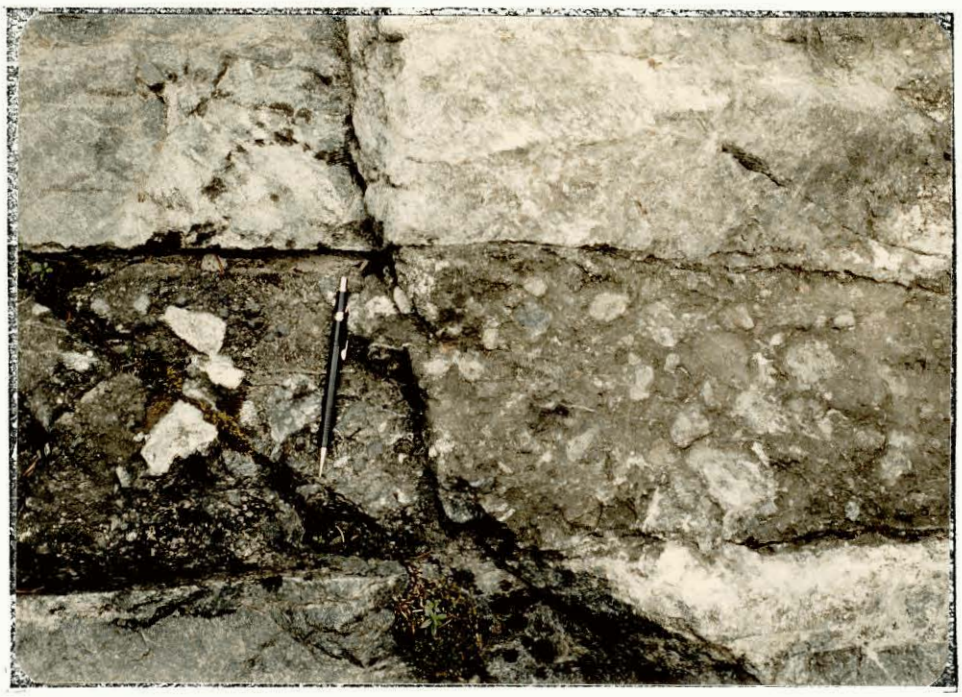

Figure 36

Lamprophyre dike in syenite breccia, Aquila Ridge. Such dikes are common near the south end of the Aquila Ridge igneous rocks.

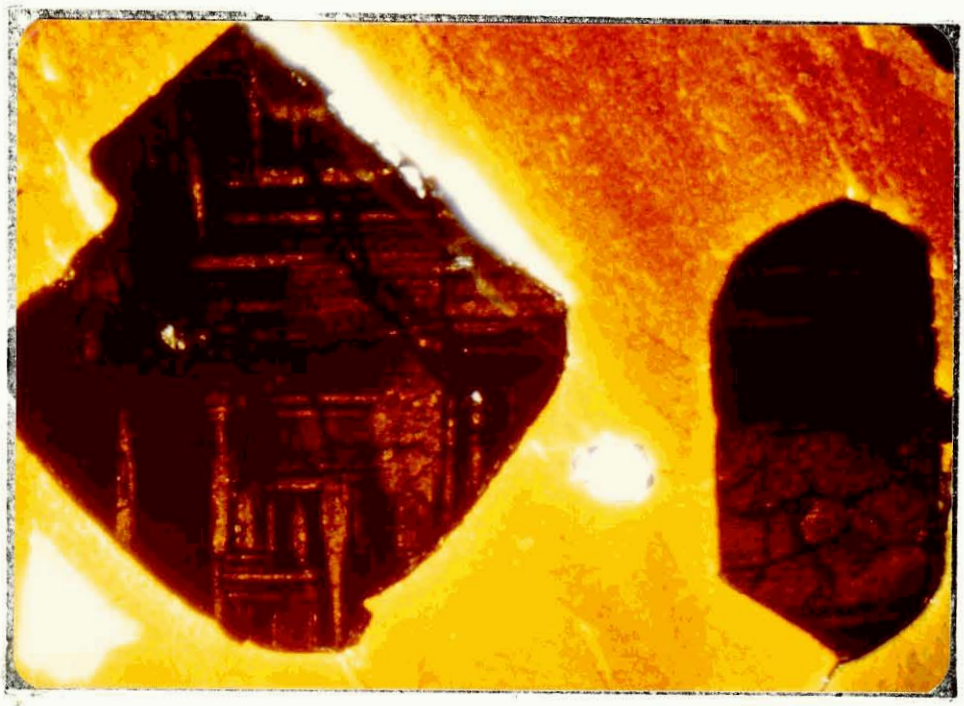

Figure 37

Euhedral perovskite in phlogopite (81-IR-6). The complex lamellar twinning is ubiquitous in all perovskites. The elongated crystal also contains a simple twin. Crossed polars.

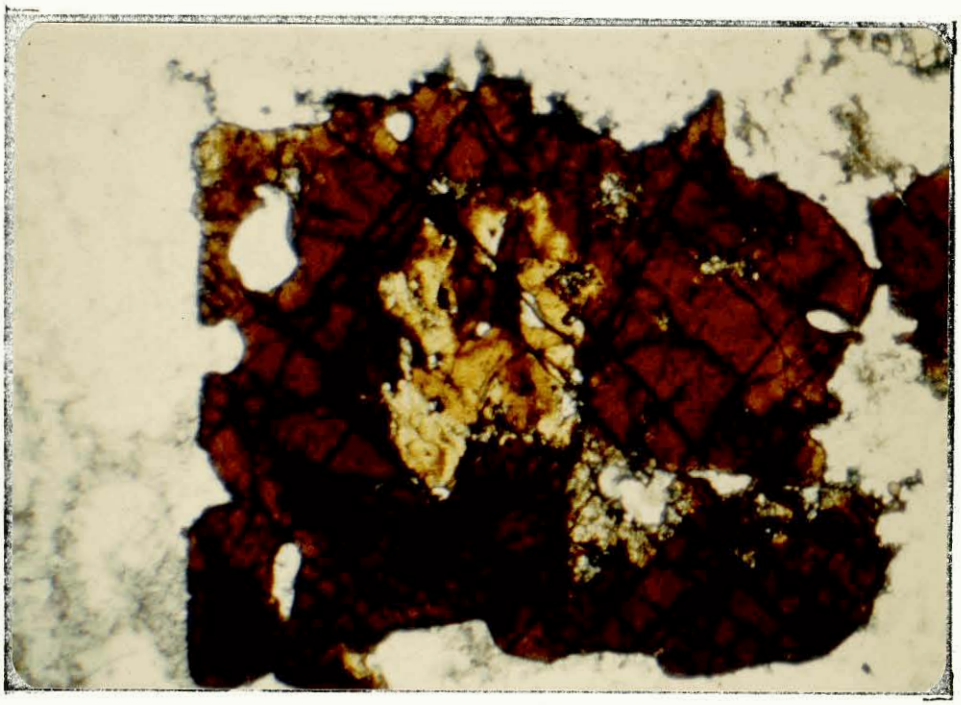

Figure 38

Melanite in nepheline syenite (81-IR-13C). This golden brown melanite contrasts strongly with the purple-red to opaque mineral of the ultramafic rocks.